AIAA JOURNAL
Vol. 50, No. 11, November 2012

Simulation and Cryogenic Experiments of Natural Convection for the Titan Montgolfiere

Yuri Feldman* and Tim Colonius†
California Institute of Technology, Pasadena, California 91125
and
Michael T. Pauken,‡ Jeffrey L. Hall,§ and Jack A. Jones¶
Jet Propulsion Laboratory, California Institute of Technology, Pasadena, California 91109

DOI: 10.2514/1.J051672

Natural convection in a spherical geometry is considered for prediction of the buoyancy of single- and double-walled balloons in a cryogenic environment such as Titan's atmosphere. The steady-state flow characteristics obtained by solving the Reynolds-averaged Navier–Stokes equations with a standard turbulence model are used to determine the net buoyancy as a function of heat input. Thermal radiation effects are shown to have a minor impact on the buoyancy, as would be expected at cryogenic conditions. The predicted buoyancy and temperature fields compare favorably with experiments preformed on a 1-m-diameter Montgolfiere prototype in a cryogenic facility. In addition, both numerical and experimental results were compared with correlations for the heat transfer coefficients for free convection internal and external to the balloon as well as in the concentric gap of the double-walled balloons. Finally, scaling issues related to inferring the performance of the full-scale Montgolfiere from the model-scale results are examined.

Nomenclature

B	=	buoyancy
$\tilde{B}$	=	nondimensional buoyancy
C	=	constant in Sutherland's law
D	=	diameter
g	=	gravitational acceleration
h	=	convection coefficient
k	=	thermal conductivity
L	=	gap width
M	=	molar mass
Nu	=	Nusselt number
Pr	=	Prandtl number
$\dot{Q}$	=	heat input
$\tilde{Q}$	=	nondimensional heat input
R	=	universal gas constant
Ra	=	Rayleigh number
Ra^*	=	modified Rayleigh number
T	=	temperature
ϵ	=	surface emissivity
μ	=	dynamic viscosity
ν	=	kinematic viscosity
ξ	=	relative deviation between measurements
ρ	=	density
σ	=	Stefan–Boltzman constant
ϕ	=	ratio of inner diameter to outer diameter

Subscripts

b	=	balloon
eff	=	effective
ext	=	external
g	=	gap
i	=	inner
int	=	internal
o	=	outer
rad	=	radiation
sim	=	simulation

Presented at the 19th AIAA Lighter-Than-Air Technology Conference, Virginia Beach, VA, September 20–22, 2011; received 12 October 2011; revision received 20 March 2012; accepted for publication 22 March 2012.

*Postdoctoral Scholar, Mechanical Engineering. Member AIAA.
†Professor, Mechanical Engineering. Associate Fellow AIAA.
‡Senior Engineer, Fluid and Thermal Systems. Senior Member AIAA.
§Senior Engineer, Mobility and Robotic Systems. Senior Member AIAA.
¶Principal Engineer, Advanced Technology. Member AIAA.

I. Introduction

IT is believed that the thick, dense nitrogen environment of Saturn's moon Titan hosts chemistry similar to prebiotic conditions on Earth. A joint NASA/ESA proposal for a follow-up to the highly successful Cassini–Huygens mission envisions a long-duration survey of Titan's surface [1]. The pros and cons of various aerial platforms for such a mission are discussed in recent articles [2–5]. Among the options, a hot-air balloon (Montgolfiere) has long been considered an attractive concept [6]. Low gravity (1/7 of Earth) and temperature (93 K at the surface) are desirable for the Montgolfiere because they reduce convective heat transfer and nearly eliminate radiation losses, respectively. Estimates show that a 2 kW heat source would be sufficient to float a payload around 200 kg [2,7]; the heat input for a comparable mass in Earth's atmosphere is about 100 times larger. Although a variety of techniques could be considered to improve the efficiency of a Montgolfiere, the insulating air gap provided by a double-walled design is simple and effective means of increasing the buoyancy for a given heat input [2].

To increase the technical readiness of a Titan Montgolfiere, estimates for the convective heat transfer need to be carefully validated, a task that is experimentally challenging due to the large-scale (roughly 10-m-diam) and low-gravity cryogenic conditions of Titan. For experiments in the terrestrial environment, it is not possible to achieve full similarity with a proposed Titanic mission [7], and compromises must therefore be made between subscale experiments at cryogenic conditions and full-scale testing at normal temperatures. For the latter case, thermal radiation losses must also be carefully estimated and isolated to translate the results to cryogenic conditions. Computational fluid dynamics (CFD) is a potentially useful predictive tool in this regard, but again, for the Titan Montgolfiere, a three-dimensional analysis that fully resolves the unsteady, turbulent convection is unfeasible because of the CPU requirements. Turbulence modeling is required.

In our previous study [7], computational models using Reynolds-averaged Navier–Stokes equations were developed to predict the natural convection heat transfer and buoyancy for an idealized balloon. The CFD models demonstrated reasonable agreement with limited experimental data and revealed some limitations of idealized engineering correlations, which tended to overpredict buoyancy in comparison with experimental and numerical results. The results motivated a new round of experiments aimed at generating more extensive data for validation, refined CFD models that account for temperature dependent fluid properties (which are important at model scale), and more-closely matched conditions between experiment and simulation. The present paper reports on this effort and is organized as follows. Section II describes the experimental set up and methodology. Section III details the basic assumptions of the numerical simulations. Section IV describes semi-analytical calculations based on the heat-transfer correlations to which both computational and experimental data are later compared in Sec. V. Finally, scaling analysis aimed at extrapolating the present model-scale results to the full-scale Titan Montgolfiere is presented in Sec. VI.

II. Experimental Setup

Two prototype balloons were tested at cryogenic temperatures covering the temperature range found in Titan's atmosphere. The balloons had a sphere-on-cone shape with a nominal diameter of 1 m. The double-walled balloon had a 5 cm gap between the inner and outer walls, or $\phi = D_i/D_0 = 0.9$. The volumes and surface areas of the fully inflated balloons, measured by photogrammetry, were smaller than those of a 1-m diameter sphere by 3 and 7%, respectively, for the single-walled balloon, and by 10 and 15%, respectively, for the double-walled balloon. The balloons were made buoyant by heating the gas with an electrical resistance heater, and voltage and current to the heater were measured to determine the power input to the balloon. The balloons were instrumented with thermocouples embedded within the walls to measure skin temperature at several locations from crown to base. The gas temperature inside the balloons was also measured in two locations. The balloons were anchored by wires to a load cell, and the net lift force was calculated by subtracting the weight of the balloon and the thermocouple setup from the load cell readings. The effect of the anchoring wires on the lift was neglected because their weight was of the same order of magnitude with the load cell precision. The load cell was placed inside a heated and insulated container to ensure it remained close to room temperature during the test.

A schematic of the cryogenic test facility is shown in Fig. 1. The cryogenic chamber sprays liquid nitrogen through a circulation fan within the chamber. A steel cylindrical shell was placed within the cryogenic chamber to provide a quiet atmosphere around the balloon during testing. Thermocouples were placed on a grid inside the cylindrical shell to measure the gas temperature around the balloon. The temperature of the cylindrical shell wall was also measured because it provides a boundary condition for the numerical simulations discussed later. Two cameras and several lights were located within the cylindrical shell to observe and record the behavior of the balloon during the test. A screenshot of the double-wall balloon inside the chamber from the down-looking camera is shown in Fig. 2. Testing each balloon first required heating them at ambient conditions to make them buoyant. Once the balloon was inflated, the cylindrical shell surrounding the balloon was closed. The cryogenic chamber was also closed, and cooling was started. The balloon heater power was reduced to the lowest heater set point during the cooldown period. After the chamber reached its first operating temperature, the heat input to the balloon was stepped through different power levels until equilibrium conditions were obtained for several different settings of heater power level. In some cases, redundant measurements were made by reducing heater power after reaching the highest level to check for repeatability or hysteresis. Equilibrium conditions were assumed to be achieved when the chamber temperature was maintained within ± 5 K of the target set point, and internal temperatures varied less than ± 1 K over a 10 min period. Fluctuations in buoyancy were less than 5% over the same period. After all power level settings had been tested, the balloons were tested at a second environment temperature by lowering the chamber temperature again and completing another series of measurements for each power level. The various equilibrium conditions achieved for both balloons are listed in Table 1.

It was noted during the testing that the balloons tended to oscillate slowly. This oscillation was probably a result of convection currents circulating within the shell due to the cold shell walls and the warm balloon skin. Moreover, it was observed that, for the double-walled balloon, full inflation was not achieved at some of the lower heat inputs. These issues are discussed more fully in Sec. V.

III. Numerical Simulation

Numerical simulations of the turbulent, free convection inside and around the single- and double-walled balloons were conducted using commercial CFD software, Ansys 13 [8]. As a first approximation, the balloon is modeled as a spherical shell with 1 m diameter (or a pair of concentric shells with 0.9 and 1 m diameters for the double-walled case). The balloons were placed in a rigid, uniform temperature cylinder of the same dimensions of the shield employed in the experiments. As noted previously, the experimental balloons were not exactly spherical, but their inflated shapes were not known to high certainty at the time the simulations were conducted and, as discussed next, differences associated with the slightly different

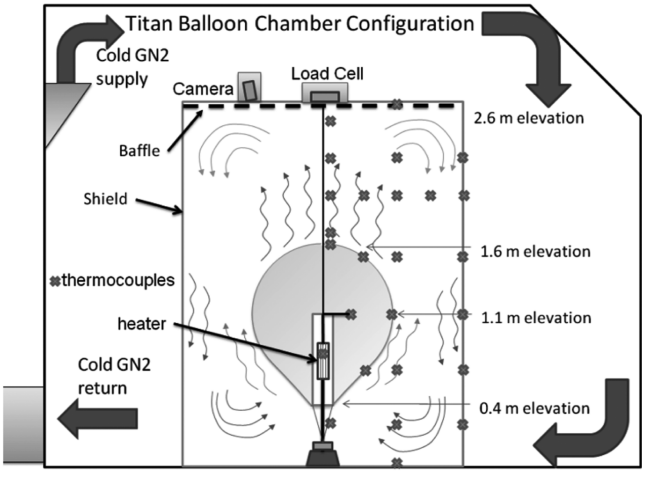

Fig. 1 Schematic description of experimental setup for a single-walled balloon.

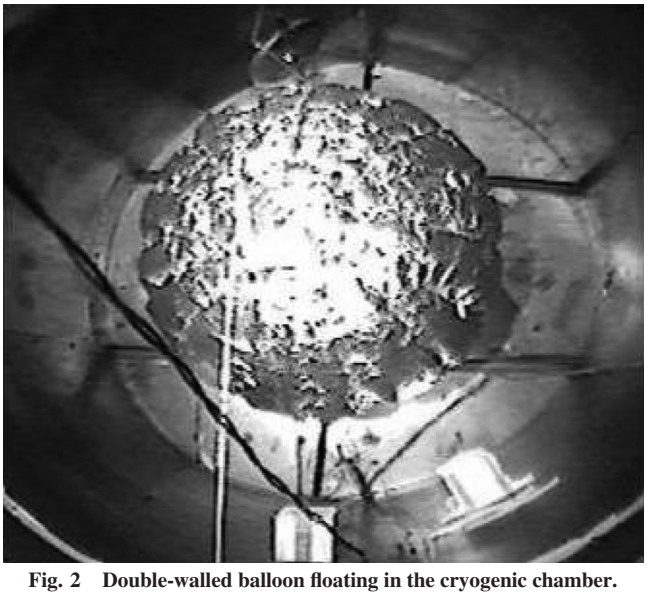

Fig. 2 Double-walled balloon floating in the cryogenic chamber.

Table 1 Experimental set points

T_∞, K					
		Single-walled $\dot{Q}$, W			
90	103	254	407	549	——
140	——	252	402	553	——
180	——	251	399	552	——
		Double-walled $\dot{Q}$, W			
90	103	254	411	546	700
140	——	266	410	550	——

shapes and sizes are likely smaller than uncertainties associated with the turbulence models.

The time-averaged turbulent flow is expected to be axisymmetric and was modeled as such. No-slip, isothermal boundary conditions were applied on the shield. The axisymmetric computational domain and a typical mesh used in the numerical simulations are shown in Fig. 3. The mesh is refined in the vicinity of the balloon boundaries. The heat source was idealized, compared to the actual strip heater in the experiments, in that the presence of fins was neglected. Instead, a uniform heat flux is specified, per unit area, on the cylindrical surface whose volume is approximately the same with that of a heat source used in the experiment. The idealization allowed us to readily investigate the influence of surface radiation effects on the balloons thermal efficiency. A surface-to-surface radiation model was used for this purpose and accounted for the mutual radiation heat transfer from all boundaries. The balloon material was aluminized Mylar with emissivity values equal to $\epsilon = 0.04$ 0.28 for the balloon/gap internal and external surfaces, respectively. The emissivity value of the heat source was estimated to be $\epsilon = 0.28$. The balloon surfaces are assumed to be perfectly conducting (negligible thickness) such that the same temperature exists on both sides of the boundary at a given location.

The Boussinesq approximation of incompressible buoyancy driven flow was employed. The approximation of incompressible flow is reasonable in the present case where the characteristic buoyancy-induced velocities are no more than 2 m/s. A more-restrictive Boussinesq approximation also assumes that temperature differences are small compared to ambient temperature, so that $(T - T_\infty)/T_\infty \ll 1$. This assumption was made in our previous modeling efforts and considerably simplifies the numerical model [7]. Although this approximation is likely very reasonable for a full-scale Titan Montgolfiere (where temperature differences are small), for the present (roughly 1/10 scale) model, $(T - T_\infty)/T_\infty$ may reach values as high as 0.43. In the present study, we therefore relaxed the second assumption and instead used the ideal gas law, simplified under the first Boussinesq approximation:

$$\rho = \frac{p_\infty M}{RT} \tag{1}$$

where p_∞ is the ambient pressure, M is the nitrogen molar mass, and R is the universal gas constant. At the same time, the nitrogen local viscosity μ and local thermal conductivity k are obtained by Sutherland's law:

$$\mu = \left(\frac{T}{T_o}\right)^{1.5} \mu_o \frac{T_o + C}{T + C} \tag{2}$$

$$k = \left(\frac{T}{T_o}\right)^{1.5} k_o \frac{T_o + C}{T + C} \tag{3}$$

where $T_o = 300.55$ K, $C = 111$ K, $\mu_o = 17.81 \times 10^{-6}$ kg/m/s, and $k_o = 17.81 \times 10^{-6}$ W/m/K.

The buoyancy is computed as

$$B = \int (\rho_\infty - \rho) g \, dV \tag{4}$$

where the densities are evaluated with Eq. (1). Based on the simulation results, the additional lift force due to the (small) hydrodynamic pressure differences and viscous shear stresses acting on the balloon were verified to be negligibly small in all cases presented here, so that, in Sec. V, the buoyancy force given by Eq. (4) is compared directly to the net lift measured in the experiments.

For the range of Rayleigh numbers achieved in the experiments, one expects fully turbulent natural convection, including thin natural convection boundary layers on the surfaces and free turbulence in the buoyant plumes rising from the heat source and the crown of the balloon. For the turbulence, a standard k–ϵ model [9] was used allowing for determination of turbulent velocity and length scales by solving two additional transport equations for kinetic energy k and dissipation rate ϵ. Standard wall functions as implemented at Ansys 13 [8] were used to resolve turbulent boundary layers at all surfaces. The spatial discretization was implemented by a second-order upwind scheme.

In all calculations that follow, a grid containing about 7×10^4 elements was used. A number of computations were also performed on denser grids containing more than 10^5 volumes. The relative differences between the buoyancy force values obtained on denser and coarser grids were less than 1%, verifying a grid independence of the results.

IV. Analytical Model

Following Samanta et al. [7], the buoyancy of the both single- and double-walled Titan Montgolfiere prototype can be estimated by applying external, gap, and internal natural convection heat transfer correlations. In these estimates, the balloon is assumed spherical, and the presence of any external boundaries such as the shield in the experiments is neglected. The correlations determine a functional dependence of the relevant Nusselt number on the corresponding Rayleigh number. Although the form of these correlations as a power law is suggested by boundary-layer theory, in turbulent convection the constants must be determined empirically from laboratory tests. It should be noted that the following correlations are based on measurements made in canonical situations where the internal, gap, and external convection are considered independently on rigid, spherical specimens, and under conditions where the surface temperature is held (approximately) uniform on all surfaces. Although such correlations are often quite accurate for the exact configurations they are intended, a significant (and not easily quantified) uncertainty is introduced in using them for the present situation where both temperature and heat flux show considerable variation over the balloon skin.

Once correlations are selected, the equations may be solved iteratively to determine the average internal temperature (and consequently the buoyancy) as a function of the heat rate. The specific correlations chosen to represent the internal, gap, and external convection are discussed in the following.

External convection and radiation: The correlation proposed by Campo [10] and verified by Wu and Jones [11] is used for the external convection. A steady-state energy balance gives

$$\dot{Q} = Nu_o \pi D_o k (T_o - T_\infty) + \sigma \pi D_o \epsilon_o (T_o^4 - T_\infty^4) \tag{5}$$

where T_o is the average temperature of the exterior balloon surface, T_∞ is the ambient temperature, and ϵ_o is the emissivity of the external balloon surface. The Nusselt number is

$$Nu_o = \begin{cases} 2 + 0.6 Ra_o^{0.25} & Ra_{D_o} < 1.5 \times 10^8, \\ 0.1 Ra_o^{0.34} & \text{otherwise} \end{cases} \tag{6}$$

and $Ra_o = Prg\beta(T_o - T_\infty)D_o^3/\nu^2$. All fluid properties are evaluated at an external film temperature $T_{of} = (T_o + T_\infty)/2$.

Convection and radiation inside the spherical gap: The correlation of Scanlan et al. [12] was used for heat transfer in the enclosure between two concentric spheres. The steady-state energy balance gives [13]

$$\dot{Q} = \mathrm{Nu}^* \pi D_o D_i k (T_i - T_o)/\delta + \sigma \pi D_i (T_i^4 - T_o^4)/(1/\epsilon_i + (1 - \epsilon_o)/\epsilon_0) \tag{7}$$

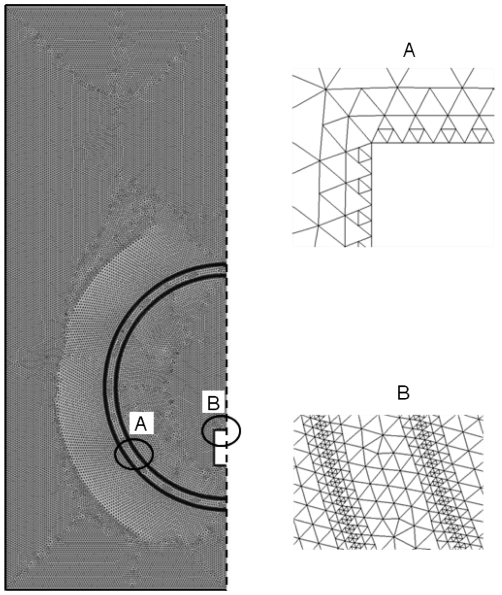

Fig. 3 Computational domain and typical discretization.

where T_i and ϵ_i are the average temperature and emissivity of the interior balloon surface, respectively, $\delta = (D_o - D_i)/2$ is the gap thickness, and the Nusselt number is given by

$$Nu^* \equiv \frac{k_{\text{eff}}}{k} = 0.228 Ra^{*0.226} \tag{8}$$

where $Ra^* = 2Prg\beta(T_i - T_o)\delta^4/(\nu^2 D_i)$. In this case, all physical properties of the flow are taken at a gap film temperature $T_{\text{gf}} = [(\bar{D}^3 - D_i^3)T_i + (D_o^3 - \bar{D}^3)T_o]/(D_o^3 - D_i^3)$, where $\bar{D} = (D_o + D_i)/2$.

Internal convection: The steady-state heat balance is

$$\dot{Q} = Nu_i \pi D_i k(T_b - T_i) + \sigma \pi D_i \epsilon_i (T_b^4 - T_i^4) \tag{9}$$

where T_b is the average temperature of the gas interior tot he balloon, and the correlation of Carlson and Horn [14] gives

$$Nu_i = \begin{cases} 2.5(2 + 0.6Ra_i^{0.25}) & Ra_i < 1.35 \times 10^8, \\ 0.325Ra_i^{0.333} & \text{otherwise} \end{cases} \tag{10}$$

where $Ra_i = Prg\beta(T_i - T_\infty)D_i^3/\nu^2$. Properties of nitrogen are taken at the interior film temperature $T_{\text{if}} = (T_i + T_b)/2$. The aforementioned approach does not include an explicit modeling of the heat source whose thermal radiation heat transfer is predicted on the basis of the balloon interior averaged temperature T_b, which is less than the heat source surface temperature, and therefore yields an underestimate of the radiation.

With the given value of $\dot{Q}$, these nonlinear equations can be solved numerically to evaluate, in turn, T_o, T_i, and T_b. Note that, to predict the buoyancy of a single-walled balloon, only steps 1 and 3 are used, whereas $T_o \equiv T_i \equiv T_g$. The nitrogen density ρ is then calculated using the ideal gas law while Sutherland's law was used to calculate the dynamic viscosity μ and thermal conductivity k at different temperatures. Tabulated values were used to find the specific heat c_p. The average density values of the internal sphere and the gap determine the overall balloon buoyancy:

$$B = \frac{\pi}{6} g[D_i^3(\rho_g - \rho_b) + D_o^3(\rho_\infty - \rho_g)] \tag{11}$$

V. Results and Discussion

A. Qualitative Flow Features

The simulated temperature distribution and stream function for the single- and double-walled balloons are shown in Fig. 4 for a typical case with $T_\infty = 90$ K and a heat input of $\dot{Q} = 550$ W. The internal flow structure is characterized by plumes, convection cells, and (momentum and thermal) boundary layers. An internal plume is formed adjacent to a heating element and rises along the centerline of the balloon, and an external plume is formed above the crown. In this time-averaged turbulent flow, a single recirculating convection cell (of toroidal shape) forms within the inner sphere. The recirculation is faster at the top. One can also distinguish the existence of a cell in the gap for the double-walled case. Very thin momentum and thermal boundary layers close to the surfaces are evidenced by the nearly discontinuous temperature field (on the scale of the plot) adjacent to the surfaces. The largest convective velocities occur where the streamlines are closest together; this occurs on both internal and external surfaces adjacent to the intense part of the internal convection cell. As expected, the insulating effect of the gap leads to a higher average temperature in the double-walled balloon compared to the single-walled case with the same ambient temperature and heat input.

B. Single-Walled Balloon Buoyancy

Figure 5 presents a comparison between experimental, numerical, and correlation values of the single-walled balloon buoyancy. In these comparisons, radiation heat transfer is switched off. Error bars on experimental data represent 3σ limits, where σ is the standard deviation of the load cell data. There is good agreement between the numerical and experimental results for the entire range of ambient temperatures and heat inputs. Discrepancy between the results is larger for higher heat transfer rates between the balloon and the surroundings. The discrepancy increases as the ambient temperature decreases and reaches its maximum (about 10%) at $T_\infty = 90$ K. The

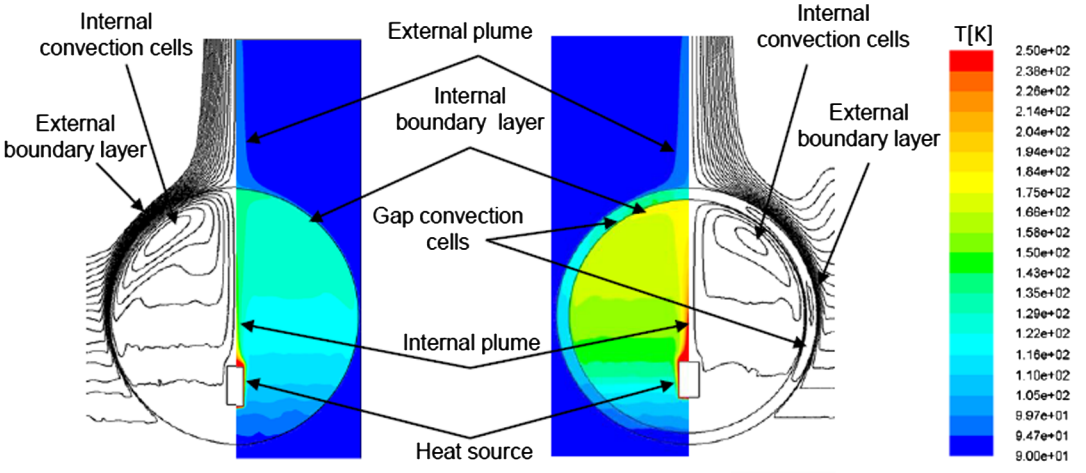

Fig. 4 Temperature and stream function distributions inside a) single-walled balloon, and b) double-walled balloon; $T_\infty = 90$ K, $\dot{Q} = 550$ W.

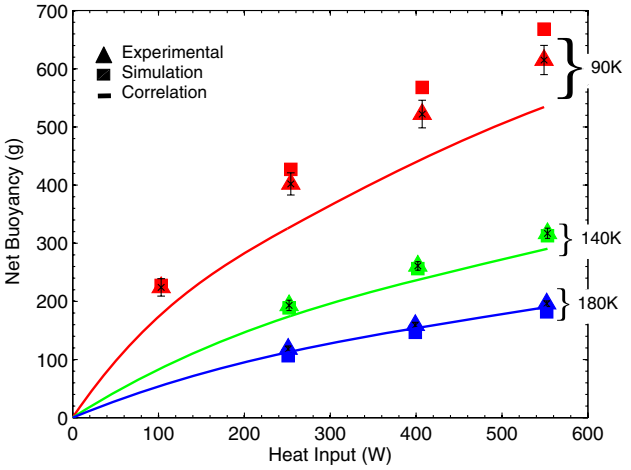

Fig. 5 Net buoyancy of the single-walled 1 m balloon.

same trend is observed for the results obtained by using empirical correlations [Eqs. (6) and (10)], which in general underestimate the buoyancy. The maximal discrepancy between the correlated and numerical buoyancy values is about 20%, when $\dot{Q} = 550$ W and $T_\infty = 90$ K. Underestimated buoyancy values obtained with empirical correlations for a single-walled balloon were also observed by Samanta et al. [7]. Accounting for the 3 and 7% smaller surface area and volume, respectively, of the experimental balloon compared to the simulated one would result in a better match of the computational and experimental data but a greater discrepancy with the correlation.

C. Double-Walled Balloon Buoyancy

Figure 6 compares experimental, numerical, and correlation values of buoyancy for the double-walled balloon. As has been already mentioned, the double-walled balloon is characterized by a superior thermal efficiency due to the insulating effect of the gap between internal and external spheres. In fact, for the entire range of the ambient temperatures and heat inputs, the buoyancy of the double-walled balloon is at least 25% more (in both experiments and simulations) than that obtained for the corresponding configuration of a single-walled balloon. As for the case of the single-walled balloon, error bars on experimental graphs represent $\pm 3\sigma$, where once again σ is the variance of the load cell measurements. Note that the values of σ are much smaller than those for a single-walled one. This may be a result of an insulating effect of the gap resulting in higher and more evenly distributed temperature inside the balloon and by this means stabilizing the internal convective flow. Similar to the single-walled balloon configuration, there is good agreement

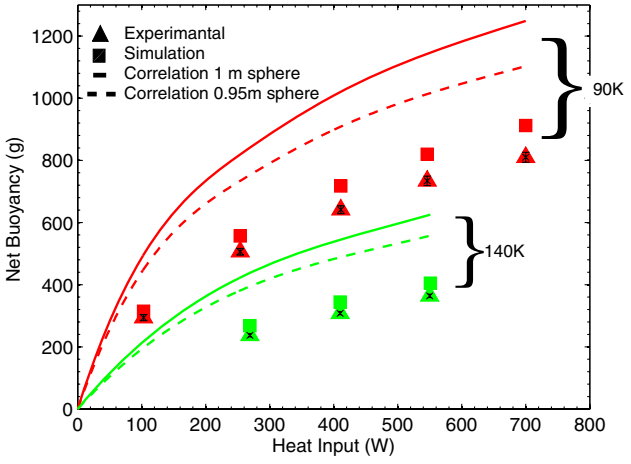

Fig. 6 Net buoyancy of the double-walled 1 m balloon.

between numerical and experimental values of buoyancy; the differences tend to increase, with the heat input reaching about 10% at $T_\infty = 90$ K and $\dot{Q} = 700$ W. Similar to the single-walled case, some of the difference between the experimental and simulated results may be due to the larger volumes and surfaces areas of the actual balloons as compared to the ideal spheres.

By contrast with the single-walled case, however, the empirical correlations now overestimate the buoyancy values by as much as 30%, compared to the experimental values. Part of this discrepancy is related to the smaller surface area and volume of the actual balloon as compared to the idealized sphere. To gauge the magnitude of this effect, we recomputed the correlations using an effective spherical outer diameter of 0.95 m (still with $\phi = 0.9$), the results of which are shown by the dashed line in Fig. 6. Although this brings the correlation closer to the data, there remains a 20% overprediction, which is especially troubling in light of the underprediction of the single-walled results. Clearly, there must be an overprediction of the insulating properties of the gap inherent in Eq. (8).

To investigate the gap correlation, the simulation results are used to evaluate the local values of temperature and heat flux at each point on both surfaces. These values are then averaged over the surfaces and converted to nondimensional values of Nusselt and Rayleigh numbers. The results are shown in Fig. 7a. Also plotted is the gap correlation due to Scanlan [12], Eq. (8), which is based on measurements of the gap between two spheres heated to uniform temperature. It can be seen that, for a scaled balloon experiment, the correlation based on a uniform surface temperature yields considerable smaller values of the effective gap conductivity than the CFD results.** The lower conductivity values overestimate the insulating effect of the gap resulting in overpredicted buoyancy values. In addition, temperature distribution along the both internal and external boundaries of the scaled balloon is far from being uniform as demonstrated in Fig. 7b, where the local temperature relative to the surface-averaged temperature is plotted along the balloon surface. Although the simulation results collapse fairly well on a power-law relation between k_{eff}/k and Ra^*, we do not recommend extrapolating this relation for use in predicting full-scale balloon gap convection because, at a larger scale, temperature nonuniformity is not as significant as it is at small scale.

Finally, in Fig. 8, we present results for the buoyancy for simulations where ϕ was varied between 0.85 and 1. These calculations show that there is a (slight) decrease in buoyancy when the gap is sufficiently large; $\phi = 0.9$ appears to be close to an optimal value, in agreement with the previous study of Samanta et al. [7].

D. Radiation Effects

Although radiation is expected to lead to a small portion of the overall heat flux at full-scale cryogenic conditions, its modeling is included in this study for two reasons. First, it is unclear that it is negligible in the small-scale experiments, where the temperature differences are much larger. In addition, adding the surface-to-surface radiation model to the CFD would enable its future use for terrestrial balloons at normal temperatures. As discussed previously, radiation was modeled in the CFD using a surface-to-surface radiation model with constant emissivities specified for the heat source, balloon fabric, and outer shield. It should be noted, however, that the surface area of a real heat source is not cylindrical and contains numerous fins. Thus, for the same heat power, the surface temperature of the heating element in the numerical simulations is higher than in the real experiment, consequently overestimating radiation heat transfer between the heating element and the internal balloon skin. Including radiation in the engineering correlations is also straightforward, except that the radiation interaction between the heat source and the inner surface of the balloon cannot be modeled directly because the former is idealized as a constant thermal output

**It is interesting to note that the direct numerical simulations of Scurtu et al. [15] of the spherical gap with constant temperature surfaces at moderate Rayleigh numbers around 2×10^5 also show a 15% higher effective conductivity compared to the Scanlan correlation [Eq. (8)].

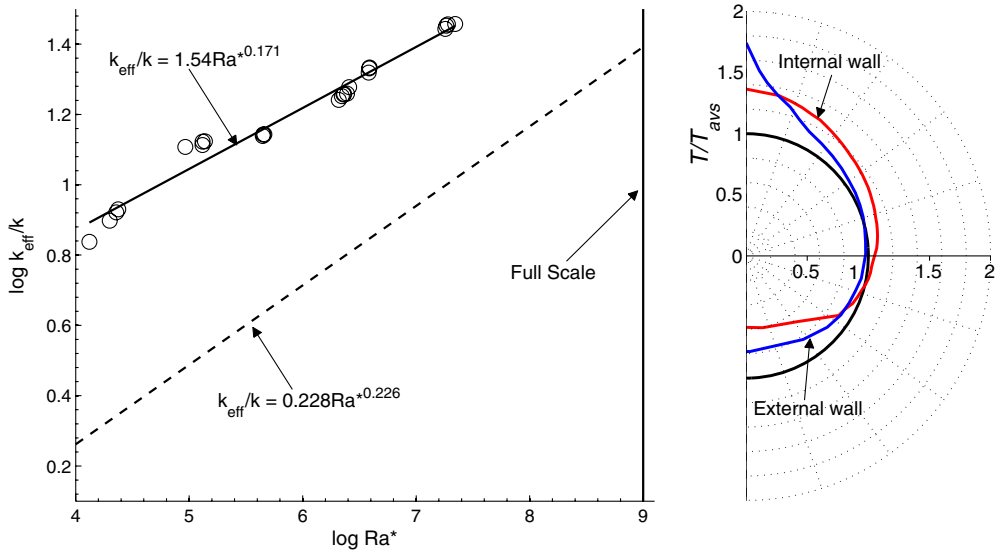

Fig. 7 Spherical gap analysis: a) comparison between and Eq. (8); b) temperature distribution, normalized by the average temperature T_{avs} of the corresponding surface, at $T_\infty = 90$ K and $\dot{Q} = 700$ W.

with no physical surface. We thus expect an underestimation of the radiation heat transfer when using correlations.

For the present cryogenic operating conditions, our numerical calculations show that the radiation heat fluxes comprise at most 5% of the overall heat input for both single- and double-walled balloons, which has a negligible (no more then 2%) effect on the overall buoyancy. We note in passing that the addition of the radiation model brings the simulations and experiments into closer agreement, but given the small magnitude it is unclear that it is significant to within the uncertainty associated with the turbulence model.

E. Local Temperature Distribution

The individual temperatures recorded by the thermocouples distributed throughout the gas and balloon surfaces are now compared. Thermocouples were placed in a single plane through the vertical centerline of the balloon at locations shown in Fig. 9. To quantify the differences between the experiments and simulations, the deviation between the measurements are defined by

$$\xi = (T_{\text{sim}} - T_{\text{exp}})/(T_{25} - T_\infty) \tag{12}$$

The deviation was normalized by the temperature at thermocouple 25 because this location generally gives the highest temperature with the exception of the one mounted adjacent to the heater. This provides a uniform comparison of the relative differences seen across all thermocouple positions. Deviation defined with respect to each individual thermocouple, of course, shows larger values for those thermocouples reading close to ambient temperature. However, because the experimental ambient temperature was not held precisely constant during the experiment, it is believed that defining deviations with respect to the maximum temperature difference across the thermocouples gives rise to simpler interpretation of the data. Thermocouples accuracy is estimated as 1 K and is not expected to introduce significant uncertainties in the following comparisons. The comparisons are shown in Fig. 10 for the operating points where ambient temperature was 90 K. Generally, deviations for the other ambient temperatures were smaller than those at 90 K but lead to similar overall conclusions. In the figure, thermocouples were grouped by balloon type (single or double), heat input, and whether

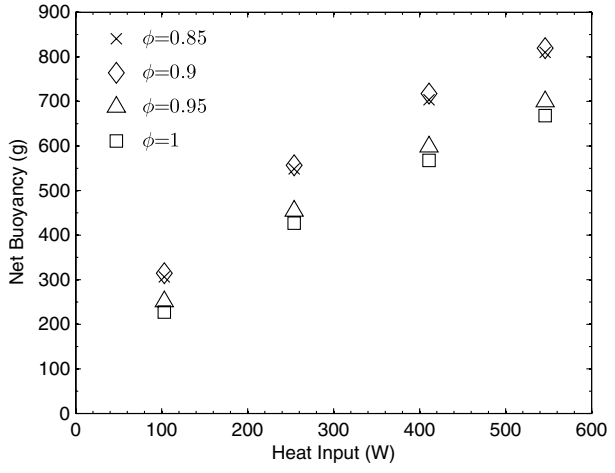

Fig. 8 Net buoyancy vs heat input for different gap widths, 1-m-diameter (external) balloon.

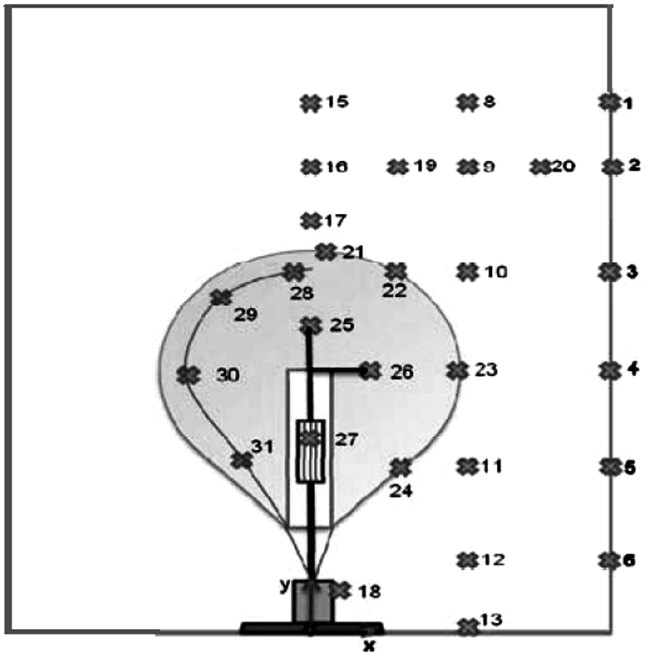

Fig. 9 Schematic of the thermocouple locations in a single- and double-walled balloon.

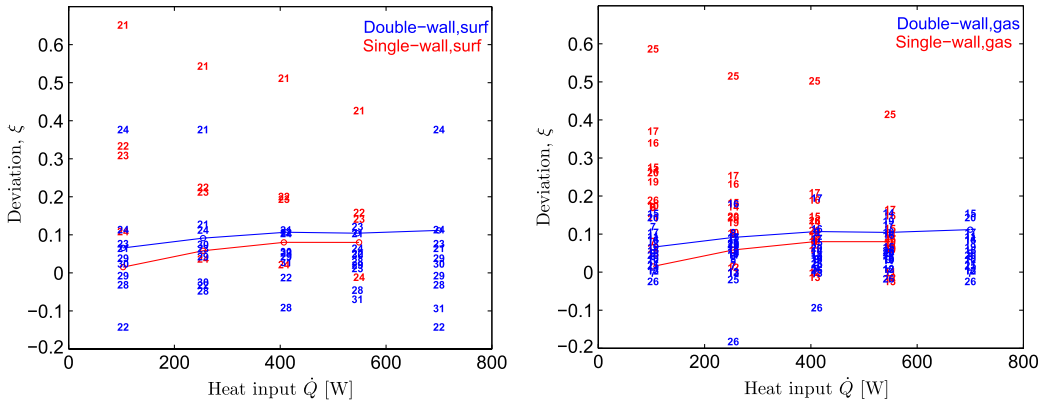

Fig. 10 Relative temperature deviation between numerical and experimental local temperatures.

the thermocouple was position in the gas or on the surface of the balloon. The majority of cases show deviations between experiment and simulation between about −5% and +15%. The differences are somewhat larger than those in net buoyancy, which are superposed on the plots (solid lines). For all values of heat input, the simulated balloon is generally hotter than the corresponding experiment, and so it is expected that corresponding thermocouple deviations will mostly be positive. The net buoyancy is approximately proportional to the difference between balloon-volume-averaged and ambient temperatures. Therefore, a larger scatter in the deviation of the pointwise temperature field than in the net buoyancy was quite expected.

Regarding those positions showing larger deviations between experiment and simulation, some trends are evident in the plots. The scatter is generally reduced as the heat input is increased, which is expected because the corresponding difference with ambient temperature simultaneously becomes larger. The largest discrepancies occur for the single-walled balloon, but for either case significant positive deviations occur in the hot plume above the heat source (25), the balloon crown (21), the hot plume above the balloon (17), and to a lesser extent at the other surface positions (22–24). Apparently, the narrow plume above the heat source is significantly hotter in simulations than in experiments. The discrepancy can be apparently attributed to some unintended motion of the balloon, which was evident in videos taken during the experiments. The motion was sufficiently slow such that it was not expected to result in any significant forced convection, but the consequent meandering of the thin plume emanating from the heater and balloon top may have caused thermocouples near the plume to be periodically exposed to the plume and to lower temperature fluid outside the plume. Likewise, turbulent convection in plumes tends also to be highly unsteady with large-scale instabilities (similar to those that are readily observed in the tip of a lit cigarette). One might expect that uncertainties in both the turbulence model to be largest at these locations. Given that the plume itself occupies a relatively small portion of the balloon volume, these larger deviations apparently do not translate into significant deviations in the net buoyancy.

Regarding the larger temperature deviations occurring at other surface positions, these may also indicate larger uncertainties in the turbulence modeling of the very thin, turbulent boundary layers. The boundary layers are predicted using a standard wall model, which does not resolve the inner details of the turbulent boundary layer. Correspondingly, there are relatively large temperature gradients across computational cells comprising the boundary.

Significant negative deviations are seen for the double-walled balloon at thermocouple positions 26 (off-axis above heat source in balloon) and 22 (outer surface midway between equator and crown). Given the opposite trend in the nearby plume/centerline, this tends to indicate that heat is distributed somewhat more evenly in the experimental flow than in the simulated one.

To summarize, the comparison between experiment and simulation obtained from the thermocouple data shows deviations in the range of 5–10%. These deviations may indicate a larger uncertainty in the numerical simulations and especially parameters associated with the turbulence model than would be inferred from the relatively smaller deviations in the net buoyancy.

VI. Scaling

In this section, we discuss scaling of the net buoyancy with increasing heat input or balloon diameter to draw implications of the model-scale results on the full-scale Titan Montgolfiere. When the temperature difference between the internal gas and ambient conditions is sufficiently small, such that both radiation and temperature-dependence of fluid properties can be neglected, the strong Boussinesq approximation (see the discussion in Sec. IV) may be employed, and in this case a dimensional analysis [7] shows that, for a given balloon geometry, there exists a universal relation between a nondimensional buoyancy $\tilde{B} = (6B)/(\pi\rho_\infty \nu_\infty^2)$ and a nondimensional heat input $\tilde{Q} = (gD^2Q)/(\rho_\infty c_p T_\infty \nu_\infty^3)$. The functional relationship may be estimated theoretically using the correlations discussed in Sec. IV or empirically using simulation or experimental data. Considering the specific geometry of a double-walled balloon idealized as concentric spherical shells, one could also say that

$$\tilde{B} = \text{fun}(\tilde{Q}, \phi) \tag{13}$$

This kind of universal scaling is particularly relevant to the Titan Montgolfiere because the expected diameter (10 m) and a realistically achievable heat input of 1–2 kW mean that the average internal gas temperature will be on the order of 10–20 K different from ambient temperature. The neglect of radiation and temperature-dependent fluid properties will thus lead to relative small errors in the overall buoyancy at full scale.

In Fig. 11, $\tilde{B}$ is plotted versus $\tilde{Q}$ for spherical single-walled balloons ($\phi = 1$) found by solving the empirical correlations from Sec. IV, restricted to cases where the temperature difference between the internal gas and ambient conditions is small. The data spans almost 4 and 5 decades in $\tilde{Q}$ and $\tilde{B}$, respectively, and includes, at the upper end, values commensurate with a full-scale balloon in the Titanic atmosphere. The universal curve is very close to a straight line, indicating a power-law dependence of $\tilde{B}$ on $\tilde{Q}$. Such a simple relation should prove very useful for system-level mission design studies. Next, we superpose CFD and experimental data from the present study along with the values from our previous simulations and experiments in the Titan Sky Simulator [7]. Without regard to the accuracy of the correlation-predicted universal relation, there is a reasonable collapse of all the data, which lends confidence to inferring the full-scale behavior based on model-scale results and simulations.

However, one notices some departures from nonuniversality in the small-scale experimental and simulation data, where three groups of

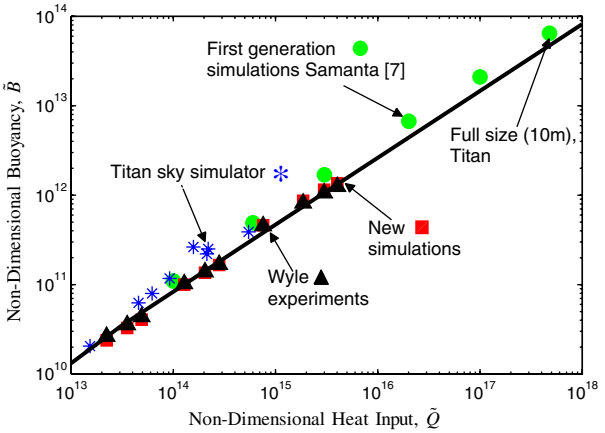

Fig. 11 Dimensionless buoyancy vs dimensionless heat input as predicted by correlations and various experimental and simulation data.

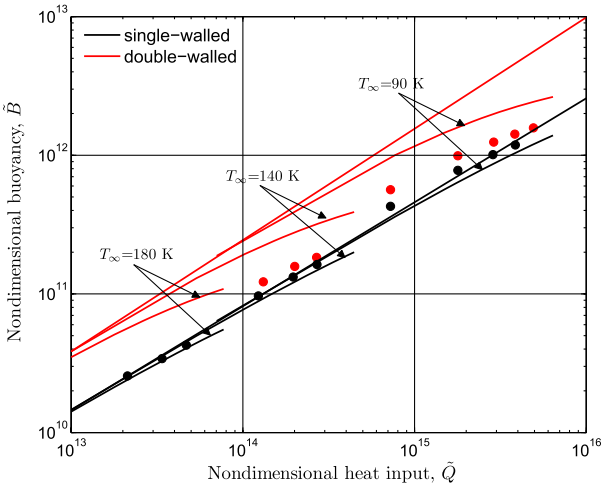

Fig. 13 Same as Fig. 12 but with present experimental data included.

points with slightly different slopes and y intercepts can be discerned. These groups correspond to the different values of T_∞ used in the experiments. This behavior occurs because, at higher temperature differences, temperature-dependent fluid properties produce a nonnegligible effect on the buoyancy, and these effects are not accounted for in the dimensional analysis leading to Eq. (13). Radiation would, if it were significant, also lead to deviations from the universal behavior, but, as was shown in Sec. V, the inclusion of radiation in the modeling leads to very small differences in buoyancy. Moreover, the previous simulations [7] assumed constant fluid properties, which explains why the buoyancy for those calculations is shifted slightly higher compared to the present ones.

These arguments are confirmed by plotting, in Fig. 12 nondimensional buoyancy versus heat input found by solving the empirical correlations of Sec. IV but including now temperature-dependent fluid properties in the calculations. Two sets of additional curves are superposed on the universal (low-temperature-difference) relations (the thick solid lines), and the families of curves are plotted for both single and double-walled balloons.

The thin solid lines are found by holding the balloon diameter and ambient temperature constant and increasing the heat input, such that the nondimensional heat input increases. One sees that, for sufficiently small nondimensional heat inputs, these lines agree with the universal behavior. However, as the heat input is increased, holding the diameter constant, the internal gas becomes hotter and buoyancy is decreased compared to the universal value. As the temperature of the gas in the balloon increases, its viscosity and thermal conductivity also increase, giving rise to a larger heat flux

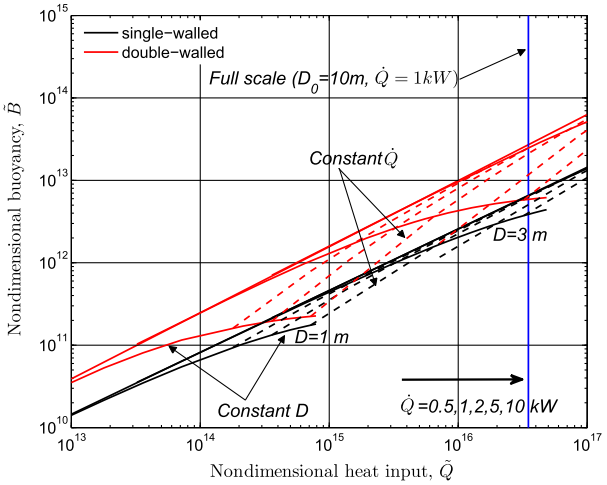

Fig. 12 Non-dimensional buoyancy versus non-dimensional heat input with temperature-dependent properties. The thick solid lines correspond to universal behavior (with constant properties).

and a lower buoyancy. Conversely, the thin dashed lines on the plot show cases where the balloon diameter is increased while holding the heat input and ambient temperature constant. In this circumstance, the nondimensional heat input still increases, but now the temperature of the gas in the balloon decreases with increasing diameter because the same amount of heat is going into a larger volume. Now the nonuniversal curves (dashed lines) approach the universal curve from below. Finally, in Fig. 13, we show curves for $D_o = 1$ m with different values of T_∞ over the range of values from the model-scale experiments and include the experimental data on the plot. Again, apart from the large discrepancy with the theoretically predicted curves, the similarity of the trends makes it clear that there are significant departures from nonuniversal behavior, owing to the hot gas temperatures reached in the small balloons.

Thus, the scaling analysis shows that there is a danger in extrapolating the small-scale experimental (or simulation) results to full scale, as it would lead to overly pessimistic buoyancy predictions. At large scale, the buoyancy penalty associated with increasing fluid viscosity and conductivity with temperature is expected to go away. For example, the present experiments and simulations for the 1 m balloon show about a 25% increase in buoyancy going from a single-walled balloon to a double-walled balloon ($\phi = 0.9$). As the insulating effect of the gap leads to even higher internal gas temperatures, the buoyancy penalty becomes even larger. At full scale, on the other hand, the insulating effect of the gap will give a larger percent increase in buoyancy for the same value of ϕ. Further simulations concentrating especially on double- or multi-walled designs at full scale are warranted and will be the topic of our future studies.

VII. Conclusions

We reported on a computational and experimental study aimed at prediction of buoyancy and temperature field of the scaled Titan Montgolfiere at terrestrial, cryogenic conditions. The numerical solutions computed by a standard k–ϵ turbulence model for an idealized spherical single- and double-walled balloon compare favorably with the corresponding results obtained experimentally. The maximum difference in net buoyancy between numerical and experimental results for both configurations is about +10%. Individual thermocouple measurements typically showed deviations, relative to the maximum temperature difference with ambient measured in each case, in the range of −5% to +15%. Larger deviations, especially for the single-walled balloons, were observed in the narrow turbulent plumes above the heater and above the balloon as well as on adjacent surfaces. For the cryogenic conditions considered here, thermal radiation effects were found to have minimal effect on the net buoyancy. Overall, the simulations thus appear to be reliable for quantitative prediction of the temperature

field and net buoyancy to within uncertainties associated with turbulence modeling, and thus the proposed model is an important step toward developing a reliable methodology for net buoyancy prediction of full-sized Titan Montgolfiere.

Given a relatively restricted amount of available heat source power (about 1.5 kW), the long-term Titan Montgolfier mission viability will benefit from a double-walled balloon design. At small scale, a 25% increase in buoyancy was achieved for the double-walled balloon compared to the single-walled balloon with the same outer diameter and heat input. However, scaling analysis, confirmed by simulation and experimental data, shows that this figure is likely pessimistic for the full-scale Montgolfiere. At this stage, we cannot confidently extrapolate a number for the gap effectivity at large-scale, due to a lack of simulation and/or experiments of double-walled balloons at full scale as well as the failure of existing heat transfer correlations for the gap effective conductivity at model scale. Thus, a main challenge for future work is to provide a more accurate heat transfer correlation for thin gaps at Rayleigh numbers commensurate with the full-scale Titan Montgolfiere. Future simulations, buoyed by the good agreement obtained here for small-scale balloons, are a promising avenue to resolve that issue.

Acknowledgments

Part of this research was carried out at the Jet Propulsion Laboratory, California Institute of Technology, under a contract with NASA. The help and support of test engineers Tim Zhang, Danh Huynh, and Phu Pham as well as technician Huan Phan at Wyle Labs, where the cryogenic testing was completed, is gratefully acknowledged. We are also thankful to Arnab Samanta and Julian Nott for their valuable advice during this project.

References

[1] Reh, K., Erd, C., Matson, D., Coustenis, A., Lunine, J., and Lebreton, J.-P., "Titan–Saturn System Mission (TSSM) Joint Summary Report," NASA and ESA, TR, 2009.

[2] Hall, J., "A Survey of Titan Balloon Concepts and Technology Status," *19th AIAA Lighter-Than-Air Systems Technology Conference*, Virginia Beach, VA, AIAA Paper 2011-6867, Sept. 2011.

[3] Lorenz, R., "A Review of Balloon Concepts for Titan," *Journal of the British Interplanetary Society*, Vol. 61, No. 1, 2008, pp. 2–13.

[4] Blamont, J., "Planetary Balloons," *Experimental Astronomy*, Vol. 22, Nos. 1–2, 2008, pp. 1–39. doi:10.1007/s10686-008-9095-8

[5] Dorrington, G., "Planetary Flight Surge Faces Budget Realities," *Advances in Space Research*, Vol. 47, No. 1, 2011, pp. 1–19. doi:10.1016/j.asr.2010.08.033

[6] Friedlander, A., "Buoyant Station Mission Concepts for Titan Exploration," *Acta Astronautica*, Vol. 14, 1986, pp. 233–242. doi:10.1016/0094-5765(86)90125-6

[7] Samanta, A., Appelo, D., Colonius, T., Nott, J., and Hall, J., "Computational Modeling and Experiments of Natural Convection for a Titan Mongolfiere," *AIAA Journal*, Vol. 48, No. 5, 2010, pp. 1007–1016. doi:10.2514/1.45854

[8] Ansys Fluent 12 Theory Guide, Ansys, Inc., Canonsburg, PA, 2009, https://www.sharcnet.ca/Software/Fluent12/html/th/node3.htm [retreived 30 Aug. 2012].

[9] Launder, B., and Spalding, D., *Lectures in Mathematical Models of Turbulence*, Academic Press, London, 1972, pp. 90–110.

[10] Campo, A., "Correlation Equation for Laminar and Turbulent Natural-Convection from Sphere," *Wärme und Stoffübertragung*, Vol. 13, Nos. 1–2, 1980, pp. 93–96. doi:10.1007/BF00997638

[11] Wu, J.-J., and Jones, J., "Performance Model for Reversible Fluid Balloons," *11th AIAA Lighter-Than-Air Systems Technology Conference*, Clearwater, FL, AIAA Paper 1995-1623, May 1995.

[12] Scanlan, J., Bishop, E., and Powe, R., "Natural Convection Heat Transfer Between Concentric Spheres," *International Journal of Heat and Mass Transfer*, Vol. 13, No. 12, 1970, pp. 1857–1872. doi:10.1016/0017-9310(70)90089-X

[13] Incropera, F., and De Witt, D., *Introduction to Heat Transfer*, Wiley, New York, 1985, p. 609.

[14] Carlson, L., and Horn, W., "New Thermal Trajectory Model for High Altitude Balloons," *Journal of Aircraft*, Vol. 20, No. 6, 1983, pp. 500–507. doi:10.2514/3.44900

[15] Scurtu, N., Futterer, B., and Egbers, C., "Three-Dimensional Natural Convection in Spherical Annuli," *Journal of Physics: Conference Series*, Vol. 137, No. 1, 2008, pp. 1–9.

T. Jackson
Associate Editor